Research Report

Structure Analysis of CeO_2-ZrO_2 Mixed Oxides as Oxygen Storage Promoters in Automotive Catalysts

Yasutaka Nagai, Takamasa Nonaka, Akihiko Suda, Masahiro Sugiura

Abstract

Oxygen storage/release (OSC) capacity is an important feature common to all three-way catalysts that enables them to efficiently remove harmful compounds such as hydrocarbons, CO and NOx in automotive exhaust gases. In this report, three types of CeO_2-ZrO_2 (Ce:Zr = 1:1 molar ratio) compounds with different OSC were characterized by means of XRD (X-ray diffraction) and XAFS (X-ray absorption fine structure). The relationship between the compounds' OSC and molecular structure was investigated by quantitative EXAFS curve-fitting analysis. Enhancing the homogeneity of the Ce and Zr atoms in the CeO_2-ZrO_2 solid solution increased OSC performance, and greatly changed the local oxygen environment around Ce and Zr. The improvement in OSC was attributed to the increase in homogeneity of the CeO_2-ZrO_2 solid solution and to the change in the oxygen environment.

Keywords Ceria, Zirconia, Oxygen storage capacity, Molecular structure, XRD, XAFS

1. Introduction

Oxygen storage/release (OSC) capacity is an important feature common to all three-way catalysts (TWCs)[1]. In TWCs, ceria is widely used as a promoter due to its high OSC based on the reversible redox reaction ($CeO_2 \leftrightarrow CeO_{2-x} + x / 2\ O_2$; x = 0 - 0.5). Ceria stores oxygen under oxygen excess conditions, and releases it under oxygen deficient conditions in order to maintain the stoichiometry. The highest catalytic performance is attained at stoichiometric conditions. However, the OSC performance and durability of pure CeO_2 are still inadequate for its use in the development of highly efficient TWCs. It has been more than ten years since our laboratory discovered that the addition of ZrO_2 to CeO_2 enhances OSC as well as thermal stability.[2, 3] Following this discovery, CeO_2-ZrO_2 has been widely utilized for commercial catalysts. A considerable number of studies have focused on the physical properties and structure of CeO_2-ZrO_2, and much has been learned on the topic.[4-7] However, the question of how the addition of ZrO_2 improves the OSC of CeO_2 remains unclear. The purpose of this study is to elucidate the relationship between the OSC and atomic structure of CeO_2-ZrO_2. Three different methods were employed to prepare three different types of CeO_2-ZrO_2 compounds having the same composition (Ce/Zr = 1). Each resultant compound exhibited a different OSC efficiency. We investigated the local structure around both Ce and Zr in these CeO_2-ZrO_2 samples using X-ray absorption fine structure (XAFS) in order to determine the cation-cation (cation = Ce, Zr) network and the oxygen environment around the cation.[8-11]

2. Experimental

2. 1 Preparation

The following three methods were utilized to prepare three types of CeO_2-ZrO_2 compounds (CZ55-1, CZ55-2 and CZ55-3), all having the same composition (Ce/Zr = 1) : CZ55-1 was prepared by precipitation with aqueous NH_3 using CeO_2 powder (Anan Kasei Co., Ltd., 99.9%, 120 m^2/g) and aqueous $ZrO(NO_3)_2$ solution. The precipitate was dried at 363 K and calcined in air at 773 K for 3 h. CZ55-2 was prepared by coprecipitation with aqueous NH_3 using aqueous $Ce(NO_3)_3$ and $ZrO(NO_3)_2$ solutions. The precipitate was dried at 363 K and calcined in air at 773 K for 3 h. CZ55-3 was synthesized by the same coprecipitation process as CZ55-2, except that the dried powder was reduced at 1473 K for 4 h in flowing pure CO and oxidized in air at 773 K for 3 h. All the samples were finally calcined in air at 773 K. Oxygen was fully stored in the Ce compounds by this treatment.

2. 2 Characterization

The oxygen storage/release capacity (OSC) was estimated by thermo-gravimetric analysis.[7] The 1 wt% platinum loaded CeO_2-ZrO_2 samples were cyclically reduced by 20% H_2 (N_2 balance) for 5 min, and then oxidized by 50% O_2 (N_2 balance) for 5 min at 773 K. The weight loss and gain were measured using a thermo-gravimetric analyzer (TGA-50, Shimadzu Corp.). The value of the weight change between the reductive and oxidative conditions corresponds to the total OSC at 773 K.

The specific surface areas of the samples were estimated using the N_2 adsorption isotherm at 77 K by the one-point Brunauer-Emmett-Teller (BET) method using an automatic surface analyzer (Micro Sorp 4232II, Micro Data Co., Ltd.). The samples were degassed in flowing N_2 at 473 K for 20 min.

Powder X-Ray diffraction (XRD) experiments were carried out using a RINT2000 (Rigaku Co., Ltd.) diffractometer with Cu-K_α radiation (1.5406 Å).

The Ce K-edge (40.45 keV) and Zr K-edge (18.00 keV) X-ray absorption fine structure (XAFS) spectra were measured at BL01B1 and BL16B2 of SPring-8 (Hyogo, Japan). The measurements were carried out using a Si (311) double crystal monochromator in transmission mode at room temperature. Data reduction of the XAFS was carried out as described elsewhere.[12] Quantitative curve-fitting analysis of the EXAFS (Extended XAFS) spectra was performed for the inverse Fourier transforms on the cation-cation (cation = Ce, Zr) and cation-oxygen shells.

3. Results and discussion

3. 1 Oxygen storage/release capacity (OSC) and BET surface area

Table 1 shows the OSC properties and BET surface area of the samples. Ce efficiency is given

by the ratio $Ce^{3+}/(Ce^{3+} + Ce^{4+})$ under reductive conditions. The Zr oxidation state in the CeO_2-ZrO_2 remains at Zr^{4+} under both the reductive and oxidative conditions at 773 K.[13] Thus, only the Ce atoms contribute to the OSC through the Ce^{3+}/Ce^{4+} redox couple. The OSC value increases in the order of CZ55-1 < CZ55-2 < CZ55-3. CZ55-3 exhibits the highest OSC, and its Ce efficiency is 88.6%. It is noteworthy that almost all of the Ce in CZ55-3 contributes to the OSC.

The BET surface areas range from 1 to 125 m^2/g (Table 1). The BET surface areas depend on the preparation methods. The BET surface area of CZ55-3 is especially low due to the high-temperature treatment during its synthesis, indicating that OSC is not related to the surface area. The number of surface oxygen atoms can be estimated to be ca. 3 μmol-O/m^2 for CeO_2-ZrO_2 (Ce:Zr = 1:1 molar ratio).[14] The experimental OSC values per m^2 of the samples were 1.3, 9.9 and 1500 μmol-O/m^2 for CZ55-1, CZ55-2 and CZ55-3, respectively. Clearly, oxygen storage/release in CZ55-1 is limited to the surface at 773 K. In the case of CZ55-2, oxygen storage/release progresses from the surface to a depth of ca. 3 layers. For CZ55-3, almost all the bulk oxygen atoms contribute to the OSC.

3. 2 XRD

Figure 1 shows the XRD patterns of the samples. The phase identification of the samples is summarized in **Table 2**. Broad XRD peaks were observed for CZ55-1 and CZ55-2, while CZ55-3 exhibited sharp peaks. CZ55-1 was shown to be a mixture of cubic CeO_2 (a = 5.41 Å) and tetragonal ZrO_2 (a = 3.58 Å, c = 5.21 Å), while CZ55-2 and CZ55-3 had a cubic structure (CZ55-2, a = 5.29 Å; CZ55-3, a = 5.26 Å). The lattice constants of the cubic phase decreased in the order of CZ55-1, CZ55-2 and CZ55-3, suggesting that the unit cell of the cubic phase shrinks in this order.

CZ55-3 mainly exhibited small peaks (indicated with an asterisk in Fig. 1), aside from the principal peaks which were attributed to the fundamental cubic fluorite type structure. The small peaks were due to the ordered arrangement of the cations.[6] It is well known that, upon high temperature reduction of CeO_2-ZrO_2, a pyrochlore-type $Ce_2Zr_2O_7$ that possesses an ordered arrangement of Ce and Zr ions forms. The κ-$Ce_{0.5}Zr_{0.5}O_2$ phase, prepared by mild-oxidation of the pyrochlore-type precursor, maintains the ordered arrangement.[6] The XRD pattern of CZ55-3 almost corresponds to that of

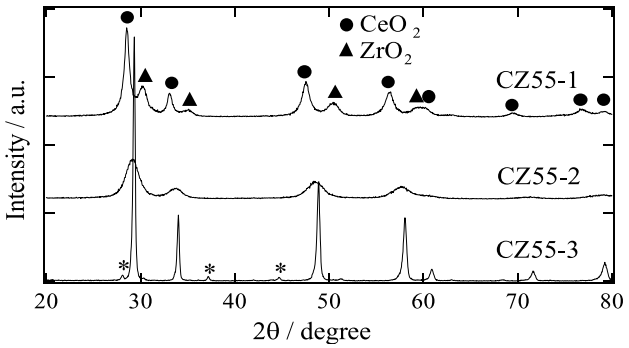

Fig. 1 X-Ray diffraction patterns of CeO_2-ZrO_2 samples having the same composition ratio (Ce/Zr = 1). Small peaks indicated with asterisks are characteristic of κ-$Ce_{0.5}Zr_{0.5}O_2$, and are a reflection of the ordered arrangement of the cations[6].

Table 1 OSC property and BET surface area of CeO_2-ZrO_2 mixed oxides.

Sample*1	OSC*2 (μmol-O/g)	Ce efficiency*3 (%)	BET surface area (m^2/g)
CZ55-1	160	9.6	125
CZ55-2	880	51.7	89
CZ55-3	1500	88.6	1

*1 : For sample description, see Experimental.
*2 : OSC (Oxygen Storage/release Capacity) of 1 wt% Pt loaded Ce compounds was measured at 773 K.
*3 : The ratio $Ce^{3+}/(Ce^{3+} + Ce^{4+})$ under reductive condition.

Table 2 Phases identified and lattice parameters determined by XRD.

Sample	Phase	Lattice parameters (Å)
CeO_2 *	Cubic	a = 5.41
CZ55-1	Cubic (CeO_2)	a = 5.41
	Tetragonal (ZrO_2)	a = 3.58 c = 5.21
CZ55-2	Cubic	a = 5.29
CZ55-3	Cubic	a = 5.26

* : Standard compound. The data refer to JCPDS cards No. 34-0394.

κ-$Ce_{0.5}Zr_{0.5}O_2$, suggesting that CZ55-3 is cubic CeO_2-ZrO_2 with an ordered arrangement of cations.

3. 3 XAFS

3. 3. 1 Fourier transforms (FTs) of Ce and Zr K-edge EXAFS spectra

FTs were performed on the Ce and Zr K-edge EXAFS spectra in roughly the 3.0 - 17 $Å^{-1}$ region. The FTs of the Ce K-edge EXAFS spectra are presented in **Fig. 2(a)**. The first peak at 1.8 Å and the second peak at 3.5 Å correspond to the Ce-O and Ce-cation (cation = Ce, Zr) bonds, respectively. The position and amplitude of the Ce-O peaks for CZ55-1, CZ55-2 and CZ55-3 are slightly different from each other. CZ55-2 and CZ55-3 exhibit lower Ce-cation peak intensities compared to CZ55-1. Also, the Ce-cation peak of CZ55-3 appears to have split in two. **Figure 2(b)** shows the FTs of the Zr K-edge EXAFS spectra. The first peak at 1.7 Å was assigned to Zr-O bonds and the second peak at 3.5 Å to Zr-cation bonds. The shape of the FTs for CZ55-1, CZ55-2 and CZ55-3 are clearly different. The results mentioned above indicate that OSC strongly correlates to the local structure around Ce and Zr.

3. 3. 2 Zr K-edge XANES (X-ray absorption near edge structure) spectra

The XANES spectra at the Zr K-edge are shown in **Fig. 3**. A careful comparison of the spectra labeled *A* and *B* across the three samples reveals several interesting facts. First, peak *A*, a weak shoulder on the steeply rising absorption edge, is more predominant in CZ55-1 and CZ55-2 than in CZ55-3. This pre-edge absorption can be assigned to the 1s $\rightarrow$ 4d transition, which is sensitive to the cation-O geometry. This transition is stronger in compounds that are distorted from centrosymmetry, considerably strong, for example, in the case of pure tetragonal ZrO_2.[15] With respect to the transition, the XANES spectra of CZ55-1 and that of pure tetragonal ZrO_2 have very similar features.[15] Furthermore, as described above, XRD revealed the presence of tetragonal ZrO_2. CZ55-2 also possesses tetragonally coordinated Zr-O bonds. On the other hand, CZ55-3 is believed to possess a Zr-O coordination of higher centrosymmetry than that of CZ55-1 or CZ55-2. The feature of the XANES spectrum of CZ55-3 is very similar to that of cubic ZrO_2.[15] As for peak *B*, it is in the form of a single broad peak in CZ55-1, while it exhibits a slight splitting in CZ55-2, and a clear splitting in CZ55-3. A similar splitting was observed for the Y_2O_3-ZrO_2 solid solution by Li et al.[16], who reported that the splitting became progressively more pronounced as the Y_2O_3 concentration increased from 3 mol% Y_2O_3-ZrO_2 (tetragonal) to 20 mol% Y_2O_3-ZrO_2 (cubic). They also observed that peak *A* decreased with increasing Y_2O_3 concentration. Thus, our XANES spectra indicate that the amount of Ce inserted into ZrO_2 increases in the order CZ55-1 < CZ55-2 < CZ55-3. Also, as more CeO_2 is inserted into the ZrO_2 lattice, the CeO_2- ZrO_2 is expected to assume a more cubic structure.

3. 3. 3 Cation-cation network

A quantitative curve-fitting analysis was performed for the cation-cation shells in the FTs to reveal the cation-cation network in the CeO_2-ZrO_2 samples. The curve-fitting results of the Ce and Zr K-edge EXAFS are summarized in **Tables 3** and **4**,

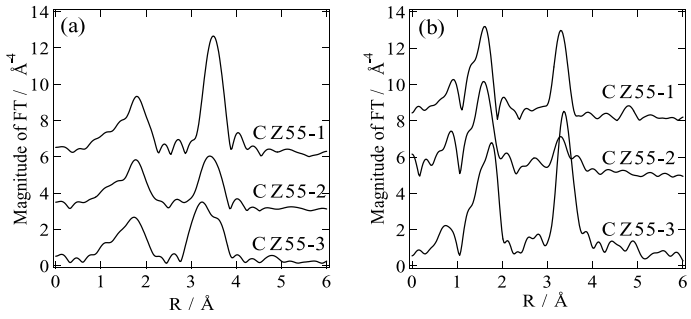

Fig. 2 Fourier-transformed κ^3x data of (a) Ce K-edge and (b) Zr K-edge EXAFS of CeO_2-ZrO_2 samples.

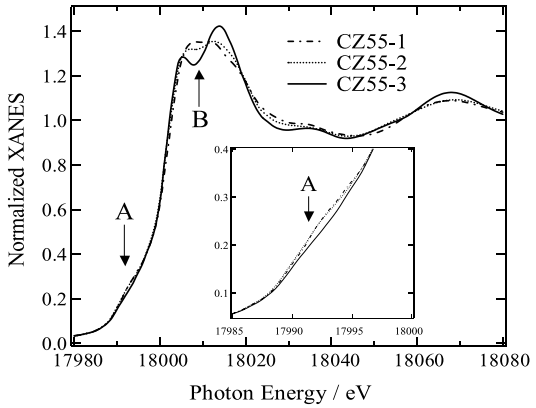

Fig. 3 Zr K-edge XANES spectra of CeO_2-ZrO_2 samples.

respectively. **Figure 4** illustrates a model for the cation-cation network, proposed based on the curve-fitting analysis results. First, the Ce-cation shell of CZ55-1 was fitted with a single Ce-Ce bond, and the Zr-cation shell was fitted with a single Zr-Zr bond. The distance (R = 3.82 Å) and coordination number (CN = 11.9) of the Ce-Ce bond are consistent with the values for CeO_2. Thus, CZ55-1 is a mixture of pure CeO_2 and ZrO_2 (Fig. 4 (a)). The CN of the Zr-Zr bond for CZ55-1 (6.6) is lower than 12. This could indicate that the size of the ZrO_2 crystallites formed was small. The average particle size was estimated from the XRD peak using the Scherrer equation. The particle size of the CeO_2 and ZrO_2 in CZ55-1 were about 130 and 80 Å, respectively. This result supports the decrease in the CN of the Zr-Zr bonds in CZ55-1. Secondly, for CZ55-2, not only Ce-Ce (Zr-Zr), but also Ce-Zr (Zr-Ce) bonds were required to obtain an appropriate fit for the cation-cation shell at the Ce (Zr) K-edge. The Ce-cation shell was fitted with Ce-Ce (CN = 8.0) and Ce- Zr (CN = 3.6) bonds. The CN of the Ce-Ce bonds is larger than that of the Ce-Zr bonds. The CN of the Ce-Zr bonds (3.6) is close to that of the Zr-Ce bonds (4.0). This indicates that, although a CeO_2-ZrO_2 solid solution does form in CZ55-2, there remain Ce- and Zr-rich domains (Fig. 4 (b)). As for the Zr-Zr bond of CZ55-2, we could not obtain an appropriate fit since the relative Debye-Waller factor ($\Delta\sigma^2$) is too large. This may mean that the distribution of the Zr-Zr bond distances is broad due to the presence of some structural disorder. Finally, the Ce-cation shell of CZ55-3 was fitted with Ce-Ce (CN = 6.0) and Ce-Zr (CN = 6.0) bonds. The Zr-cation shell was fitted with Zr-Zr (CN = 6.0) and Zr-Ce (CN = 6.0) bonds. The CN ratios of Ce-Ce to Ce-Zr and Zr-Zr to Zr-Ce are exactly 1. These CN ratios are equal to the Ce/Zr composition ratio of the sample. Clearly, the $Ce_{0.5}Zr_{0.5}O_2$ solid solution formed in CZ55-3 is homogeneous at an atomic level. Furthermore, as mentioned in the XRD section, CZ55-3 possesses an ordered arrangement of Ce and Zr ions (Fig. 4 (c)). The homogeneity of the CeO_2-ZrO_2 solid solution increases in the order of CZ55-1, CZ55-2 and CZ55-3. This is in agreement with the Zr K-edge XANES data. All

Table 3 Results of curve-fitting analysis for Ce-cation shells[*1].

Sample	Bond	CN	R (Å)	$\Delta\sigma^{2}$ [*2] (Å^2)
cubic CeO_2 [*3]	Ce-Ce	12	3.826	
CZ55-1	Ce-Ce	11.9(2)	3.82(0)	0.0026(1)
CZ55-2	Ce-Ce	8.0(4)	3.78(0)	0.0034(2)
	Ce-Zr	3.6(5)	3.71(0)	0.0063(13)
CZ55-3	Ce-Ce	6.0(3)	3.78(0)	0.0016(2)
	Ce-Zr	6.0(3)	3.72(0)	0.0022(3)

*1 : The standard deviation is given in parentheses.
*2 : Relative Debye-Waller factor
*3 : Standard compound

Table 4 Results of curve-fitting analysis for Zr-cation shells[*1].

Sample	Bond	CN	R (Å)	$\Delta\sigma^{2}$ [*2] (Å^2)
cubic CeO_2 [*3]	Zr-Zr	12	3.628	
CZ55-1	Zr-Zr	6.6(2)	3.66(0)	0.0061(1)
CZ55-2	Zr-Zr	3.0(6)	3.69(0)	0.0124(19)
	Zr-Ce	4.0(3)	3.76(0)	0.0030(3)
CZ55-3	Zr-Zr	6.0(4)	3.62(0)	0.0086(6)
	Zr-Ce	6.0(3)	3.75(0)	-0.0010(1)

*1 : The standard deviation is given in parentheses.
*2 : Relative Debye-Waller factor
*3 : 8 mol% Y-doped cubic ZrO_2 as standard compound

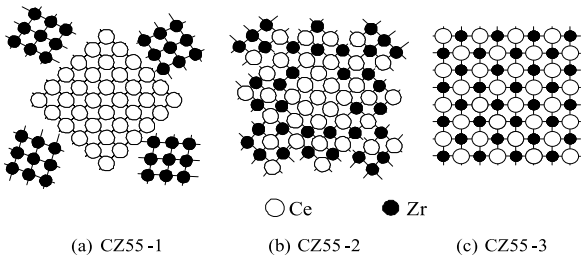

Fig. 4 Schema illustrating the cation-cation network in the CeO_2-ZrO_2 samples having the same composition (Ce/Zr = 1). CZ55-1 consists of pure CeO_2 and ZrO_2. A CeO_2-ZrO_2 solid solution forms in CZ55-2, but the Ce- and Zr-rich domains still remain. The $Ce_{0.5}Zr_{0.5}O_2$ solid solution that forms in CZ55-3 is homogeneous at atomic level, possessing an ordered arrangement of Ce and Zr ions.

these results lead to the conclusion that OSC increases by enhancing the homogeneity of the Ce and Zr atoms in the CeO_2-ZrO_2 solid solution.

3. 3. 4 Oxygen environment around cation

Tables 5 and **6** present the curve-fitting results for the Ce-oxygen and Zr-oxygen shells, respectively. The CN of Ce-O for all samples was 8. The Ce-O bond length (R = 2.33 Å) of CZ55-1 is almost consistent with that of the CeO_2 standard. The Ce-O bond length gradually shortens in the order CZ55-1 > CZ55-2 > CZ55-3. Since the CeO_2-ZrO_2 solid solution in CZ55-2 is inhomogeneous, its Ce-O bond length is the average value of all the Ce-O bonds. A model for the oxygen environment around Ce is proposed in **Fig. 5**. The differences in Ce-O bond lengths are interpreted as follows. Since the ionic radius of Zr^{4+} (0.84 Å) for an 8-fold coordination is smaller than that of Ce^{4+} (0.97 Å),[17] the unit cell of the cubic CeO_2-ZrO_2 solid solution decreases with increasing undersized Zr^{4+} concentration inserted into the Ce network, causing the Ce-O bond length to shorten. This hypothesis is further supported by the decrease in the lattice constant of the CeO_2-ZrO_2 samples.

The Zr-O bond of CZ55-1 was fitted with two sets of short and long Zr-O bond lengths. The Zr-O bond length and CN are close to the characteristic values for standard tetragonal ZrO_2.[15] The Zr-O bond of CZ55-2 also consisted of two sets of Zr-O bond lengths. However, the Zr-O CN for CZ55-2 (6 + 2) is different from that for standard tetragonal ZrO_2 (4 + 4). By contrast, the Zr-O bond for CZ55-3 was fitted with a single Zr-O bond. The model for the oxygen environment around Zr is proposed in **Fig. 6**. These

Table 5 Results of curve-fitting analysis for Ce-oxygen shells[*1].

Sample	Bond	CN	R (Å)	$\Delta\sigma^{2}$ [*2] (Å^2)
cubic CeO_2[*3]	Ce-O	8	2.343	
CZ55-1	Ce-O	8.0(1)	2.33(0)	0.0035(1)
CZ55-2	Ce-O	8.0(1)	2.30(0)	0.0052(3)
CZ55-3	Ce-O	8.0(2)	2.27(0)	0.0044(2)

*1 : The standard deviation is given in parentheses.
*2 : Relative Debye-Waller factor
*3 : Standard compound

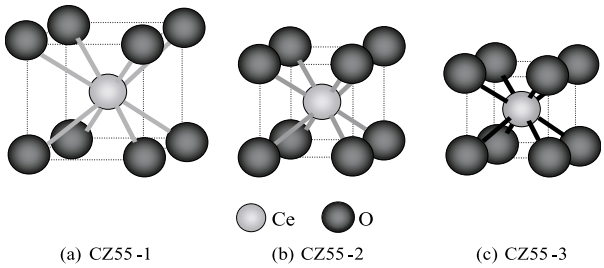

Fig. 5 Schema illustrating oxygen environment around Ce. The Ce-O bond length gradually shortens in the order CZ55-1 > CZ55-2 > CZ55-3.

Table 6 Results of curve-fitting analysis for Zr-oxygen shells[*1].

Sample	Bond	CN	R (Å)	$\Delta\sigma^{2}$ [*2] (Å^2)
cubic CeO_2[*3]	Zr-O	8	2.222	
CZ55-1	Zr-O Zr-O	4.0(5) 4.0(6)	2.17(0) 2.36(0)	-0.0081(5) 0.0067
CZ55-2	Zr-O Zr-O	6.0(5) 2.0(5)	2.19(0) 2.37(3)	-0.0059(4) -0.0017(11)
CZ55-3	Zr-O	8.0(2)	2.27(0)	-0.0046(2)

*1 : The standard deviation is given in parentheses.
*2 : Relative Debye-Waller factor
*3 : 8 mol% Y-doped cubic ZrO_2 as standard compound

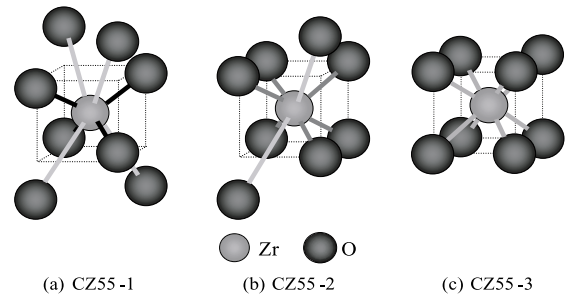

Fig. 6 Schema illustrating oxygen environment around Zr. In CZ55-1, a pure tetragonal ZrO_2 forms and has two sets of short and long Zr-O bond lengths. In CZ55-2, the Zr-O coordination is, on average, somewhat more centrosymmetric than that in tetragonal ZrO_2. The configuration of the oxygen around Zr for CZ55-3 has a hightly symmetric 8-fold coordination.

observations are interpreted as follows. In CZ55-1, a pure tetragonal ZrO_2 forms, and has two sets (4 + 4) of short and long Zr-O bond lengths. In CZ55-2, the Zr-O coordination is, on average, somewhat more centrosymmetric than that of tetragonal ZrO_2 due to the introduction of Zr ions into the cubic CeO_2 framework. Because of the inhomogeneous CeO_2-ZrO_2 solid solution in CZ55-2, Fig.6(b) represents the average structure of the oxygen environment around all Zr atoms, and is an intermediate state between CZ55-1 and CZ55-3. In CZ55-3, a cubic $Ce_{0.5}Zr_{0.5}O_2$ solid solution homogeneously forms at the atomic level. Hence, the oxygen around Zr has a rather symmetric 8-fold coordination. These results are in agreement with the Zr K-edge XANES observations that CZ55-3 possesses a higher centrosymmetry of Zr-O coordination compared to CZ55-1 and CZ55-2.

3. 4 Mechanism of OSC improvement

We discuss the mechanism of OSC improvement from the viewpoints of homogeneity and oxygen environment. The effective ionic radii of Ce^{4+}, Ce^{3+} and Zr^{4+} are 0.97, 1.14 and 0.84 Å, respectively.[17] During the oxygen release process, the volume of the Ce compound increases in proportion to the change in the Ce oxidation state from Ce^{4+} to Ce^{3+}. The stress energy arising from this volume increase would restrict any further valence change of the Ce ($Ce^{4+} \rightarrow Ce^{3+}$). The introduction of undersized Zr ions into the Ce framework could compensate for the volume increase, and ease the valence change. This would explain why the enhancement of the homogeneity of Ce and Zr atoms in the CeO_2-ZrO_2 solid solution improves OSC performance.

By the introduction of Zr ions into the cubic CeO_2 framework on an atomically homogenous level, the Ce-O bond length shortens, and the configuration of the oxygen around Zr assumes a more centrosymmetric coordination. In particular, CZ55-3 has a rather symmetric 8-fold coordination around Zr, which is generally considered to be spatially tight and unstable, because the ionic radius of Zr^{4+} (0.84 Å) is much smaller than that of O^{2-} (1.38 Å).[17] On the other hand, the oxygen environment around Ce in CZ55-3 is also considered to be tight because the Ce-O bond length in CZ55-3 is much shorter than that in the stable pure CeO_2. Actually, CZ55-3, the κ-$Ce_{0.5}Zr_{0.5}O_2$ solid solution, is not a stable phase but a metastable one in an oxidative atmosphere[5], and maintains its structure at 1273 K and below. However, if the temperature exceeds 1473 K, a phase separation occurs in the oxidative atmosphere, and CZ55-3 is partially divided into stable CeO_2 and ZrO_2. We confirmed these phenomena by XRD. This instability of the oxygen environment around Ce and Zr will generate active oxygens responsible for the improved OSC.

4. Summary

The present study clearly showed the relationship between OSC and local structure around Ce and Zr in three types of CeO_2-ZrO_2 compounds (Ce:Zr = 1:1 molar ratio). OSC increases by enhancing the homogeneity of the Ce and Zr atoms in the CeO_2-ZrO_2 solid solution. The $Ce_{0.5}Zr_{0.5}O_2$ solid solution, which is homogeneous on an atomic level, exhibited the highest OSC among these CeO_2-ZrO_2 samples. The enhancement of the homogeneity of the Ce and Zr atoms could ease the valence change of the Ce ($Ce^{4+} \rightarrow Ce^{3+}$). Upon introduction of Zr ions into the cubic CeO_2 framework on an atomically homogeneous level, the Ce-O bond length in the CeO_2-ZrO_2 shortens, and the configuration of the oxygen around Zr assumes a more centrosymmetric 8-fold coordination. This modification of the local oxygen environment around Ce and Zr will generate some active oxygens that will play a role in OSC improvement. Our conclusion is that the main contributing factors in OSC improvement are the enhancement of the homogeneity of the CeO_2-ZrO_2 solid solution and the modification of the oxygen environment.

Finally, the present study shows that the development of high performance catalysts will require catalyst design at the atomic level.

Acknowledgements

We thank Drs S. Yoshida (Kyoto Univ.), T. Tanaka (Kyoto Univ.), T. Yamamoto (Kyoto Univ.) and T. Okamoto (Chubu Univ.) for their assistance with XAFS analysis. The XAFS experiments were performed at the SPring-8 with the approval of the Japan Synchrotron Radiation Research Institute (JASRI) (Proposal No. 2000A0143-NX-np & C99B16B2-417N).

References

1) Matsumoto, S. : Toyota Tech. Rev., **44**(1994), 10
2) Ozawa, M., et al. : Japanese unexamined patent pub., 116741(1988), (in Japanese)
3) Ozawa, M., et al. : J. Alloys Comp., **193**(1993), 73
4) Vlaic, G., et al. : J. Catal., **168**(1997), 386
5) Mamotov, E., et al. : J. Phys. Chem. B, **101**(2000) 11110
6) Kishimoto, H., et al. : J. Alloys Comp., **312**(2000), 94
7) Suda, A., et al. : J. Ceram. Soc. Jpn., **109**(2001), 177
8) Nagai, Y., et al. : J. Synchrotron Rad., **8**(2001), 616
9) Nagai, Y., et al. : SPring-8 Research Frontiers 1999/2000, pp.46
10) Nagai, Y., et al. : Catal. Today, **74**(2002), 225
11) Nagai, Y., et al. : *Housyakou*, **15**(2002) 37 (in Japanese)
12) Tanaka, T., et al. : J. Chem. Soc., Farad. Trans., **84** (1988), 2987
13) Fornasiero, P., et al. : J. Catal., **151**(1995), 168
14) Tanabe, T., et al. : Stud. Surf. Sci. Catal., **138**(2001), 135
15) Li, P., et al. : Phys. Rev. B, **48**(1993), 10063
16) Li, P., et al. : Phys. Rev. B, **48**(1993), 10074
17) Shannon, R. D., et al. : Acta Cryst., **B25**(1969), 925

(Report received on Oct. 9, 2002)

Yasutaka Nagai
Year of birth : 1967
Division : Research-Domain 31
Research fields : Automotive Catalyst
Academic Society : Catal. Soc. of Jpn.

Takamasa Nonaka
Year of birth : 1972
Division : Materials Analysis Development Lab
Research fields : X-ray absorption spectroscopy
Academic society : Jpn. Soc. for Sychrotron Rad. Res., Ceram. Soc. of Jpn.

Akihiko Suda
Year of birth : 1958
Division : Research-Domain31
Research fields : Catal. Mater.
Academic society : Am. Ceram. Soc., Ceram. Soc. Jpn.

Masahiro Sugiura
Year of birth : 1942
Division : Research Administrative Planning Office, Mater.
Research fields : Automot. catal., Porous Adsorptive Mater.
Academic degree : Dr. Eng.
Academic society : Catal. Soc. Jpn., Jpn. Petroleum Inst., Chem. Soc. Jpn., Soc. Automot. Eng. Jpn., Ceram. Soc. Jpn., Jpn. Soc. Adsorption, Jpn. Soc. Diatomology
Awards : Jpn. Soc. Promot. Machine Ind. Prize, 30th (1995)